AD-A180 307 ACOUSTO-OPTIC SPECTRUM ANALYZER: TEMPORAL RESPONSE AND DETECTION OF PULSED SIGNALS(U) DEFENCE RESEARCH ESTABLISHMENT OTTAWA (ONTARIO) J P LEE DEC 86 1/1

UNCLASSIFIED DREO-TN-87-5 F/G 9/6 NL

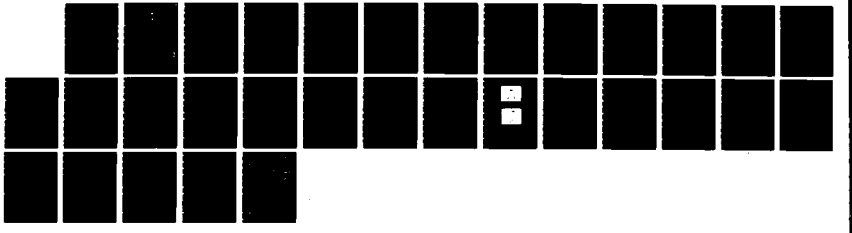

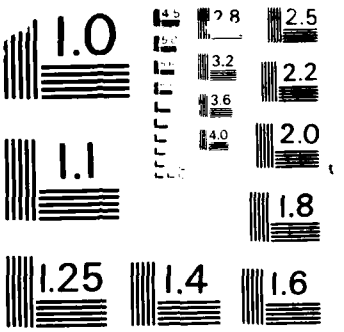

MICROCOPY RESOLUTION TEST CHAR

National Defence / Defense nationale

ACOUSTO-OPTIC SPECTRUM ANALYZER: TEMPORAL RESPONSE AND DETECTION OF PULSED SIGNALS

by

Jim Pak-Yee Lee

DEFENCE RESEARCH ESTABLISHMENT OTTAWA
TECHNICAL NOTE 87-5

Canada

December 1986
Ottawa

National Defence / Defense nationale

ACOUSTO-OPTIC SPECTRUM ANALYZER: TEMPORAL RESPONSE AND DETECTION OF PULSED SIGNALS

by

Jim Pak-Yee Lee
Radar ESM Section
Electronic Warfare Division

DEFENCE RESEARCH ESTABLISHMENT OTTAWA
TECHNICAL NOTE 87-5

PCN
011LB11

December 1986
Ottawa

ABSTRACT

This report describes the temporal response of an acousto-optic spectrum analyzer to pulse-modulated cw signals. The detected waveforms from the outputs of a real-time photodetector array are analyzed as a function of pulse width, weighting function parameters, and relative photodetector to spectral centroid location. The input pulse envelope is modified in the forms of signal duration stretching, the appearance of a flattop, multiple humps, and longer rise and fall times. Various schemes are discussed on the determination of the pulse width from the detected waveform.

RÉSUMÉ

Description de la réaction temporelle d'un analyseur de spectre acousto-optique par rapport à des signaux cw modulés par impulsions. Les formes d'ondes détectées à l'aide des sorties d'un réseau photodétecteur en temps réel sont analysées en tant que variable de l'impulsion en durée, des paramètres de la fonction de pondération et de l'emplacement relatif du photodétecteur par rapport au centre géométrique spectral. L'enveloppe de l'impulsion d'entrée est modifiée par l'accroissement de la durée du signal, l'apparition d'une amplitude courante, des dénivellations multiples et le prolongement des temps de montée et de descente. On étudie différents plans de détermination de l'impulsion en durée à l'aide de la forme d'onde détectée.

TABLE OF CONTENTS

LIST OF ILLUSTRATIONS

1.0 INTRODUCTION

The optical Fourier transforming configuration as shown in Fig.1, where a single-channel Bragg cell is employed, is an acousto-optic spectrum analyzer. This configuration is well known for its inherent capability of wideband spectrum analysis on a real-time basis with many simultaneous signals present. With the advent of new components such as Bragg cells and photodetector arrays, acousto-optic technology has rapidly emerged as a major optical signal processing technique for wideband reception and analysis of radar signals.

The acousto-optic spectrum analyzer is a real-time processor in which the output is the instantaneous Fourier transform of the weighted input signal in the aperture. The amplitude weighting function takes into account the acoustic attenuation and the interaction profile between the laser beam and the acoustic beam in the aperture. For cw signals, the spatial and temporal characteristics of the spectrum are constant and are determined by the Fourier transform of the product of the amplitude weighting function and the signal [1],[2]. On the other hand, in the case where the signal is of finite duration, such as with pulse-modulated cw signals, the instantaneous spectrum is a function of where the signal is located in the aperture and is a more complex problem [3]-[5].

A photodetector array is usually used for detecting the spectrum. The output from such a processor also depends on a number of other factors such as the number of photodetectors used to cover a given frequency band, the response of the photodetector, and whether it is operating in the time-integrating or the real-time mode.

In this report we investigate both the spatial and temporal characteristics of the acousto-optic spectrum analyzer to pulse-modulated cw signals. The formation of the temporal and spatial distributions in the Fourier plane as a pulsed signal propagates through the Bragg cell aperture is analyzed in detail. The detected signal waveform from a photodetector array operating in the real-time mode is then analyzed as a function of the pulse width, weighting function parameters, and the relative position of the photodetector to the spectral centroid. Two simple methods of determining the pulse width from the detected signal waveforms are also discussed.

2.0 SPATIAL AND TEMPORAL DISTRIBUTIONS

A Fourier transforming configuration is shown in Fig. 1, where the Bragg cell is illuminated with a collimated source of monochromatic light at the Bragg input angle. An electrical signal is applied to the transducer of the Bragg cell and a portion of the light is diffracted into one of the first-order components. The interaction between sound and light is assumed to

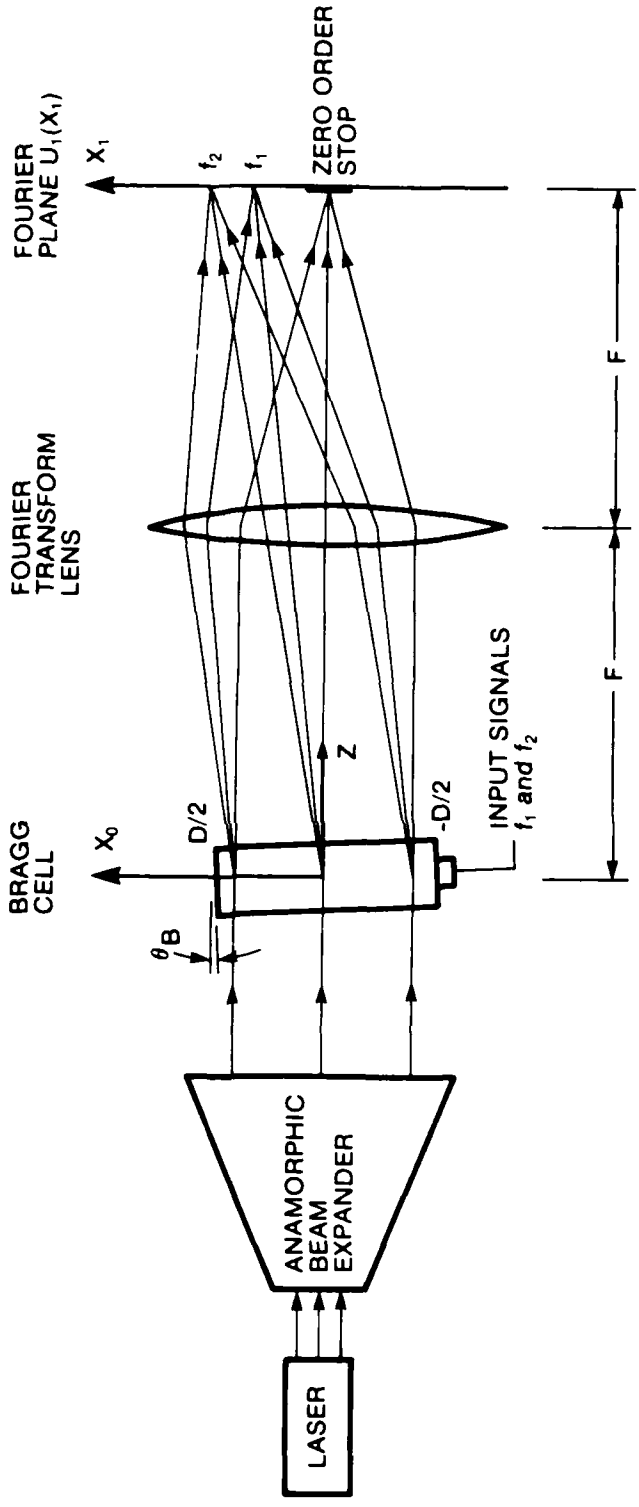

FIG. 1: SCHEMATIC DIAGRAM OF ACOUSTOOPTIC SPECTRUM ANALYSER

be ideal and the effect of the acoustic spreading in the y direction is neglected. The light amplitude distribution of the diffracted first-order component, in the back focal plane of the lens, is given by [6]

$$U_1(x_1,y_1,t) = \frac{K_B}{\lambda F} \int_{-\infty}^{\infty} g(t - x_0/v_s)\, w(x_0,y_0)$$

$$\cdot \exp[-j2\pi(ux_0 + vy_0)]\, dx_0 dy_0 , \qquad (1)$$

where

$$u = \frac{x_1}{\lambda F} , \qquad v = \frac{y_1}{\lambda F}$$

are expressed in normalized coordinates, λ is the optical wavelength, F is the focal length of the lens, K_B is a constant which is proportional to the square root of the acousto-optic diffraction efficiency of the Bragg cell and the illuminating laser power, $g(t- x_0/v_s)$ is the acoustic signal function, v_s is the acoustic velocity, and $w(x_0, y_0)$ is the amplitude window weighting function.

In the implementation of spectrum analyzers, the Bragg cell is often illuminated with a line source. The optics is configured to perform a 1-D Fourier transform in the x_1 direction and the line source is imaged in the y_1 direction. This operation is generated by inserting a cylindrical lens in front of the Bragg cell and another in between the Bragg cell and the Fourier transform lens. In this arrangement, the effects of the acoustic curvature in the y direction on the intensity distribution have been analyzed [2] and found to be small. As a result, the analysis presented in this report can be simplified by assuming the acousto-optic medium produces a self-collimating acoustic beam.

In this arrangement, the weighting function can in general be approximated by

$$w(x_0,y_0) = \mathrm{rect}\left(\frac{x_0}{D}\right) \delta(y_0) \exp\left[-\pi\left(\frac{x_0}{D} + \frac{1}{2}\right)\right]$$

$$\cdot \exp\left[-\left(2Tx\,\frac{x_0}{D}\right)^2\right]$$

$$= \text{rect}\left(\frac{x_0}{D}\right) \delta(y_0) \exp\{ /2[/(8Tx) - 1]\}$$

$$\cdot \exp\left(-\{2Tx[x_0/D + /(8Tx)]\} \right) \qquad (2)$$

where δ is the Dirac delta function, rect is the rectangular function, the input laser profile is of the Gaussian form with Tx specifying the intensity truncation ratio at the $1/e^2$ points, α is the acoustic attenuation coefficient in Np/s and increases with the input frequency, and τ is the acoustic transit time across the effective aperture D. In the latter expression of Eq.(2), both the acoustic exponential attenuation and the Gaussian illumination profile have been combined into a displaced Gaussian function.

In the case of a pulse-modulated cw signal of the form

$$V_{in}(t) = C \text{ rect}[(t - PW/2)/PW] \cos(2\pi f_s t + \phi_0), \qquad (3)$$

the corresponding acoustic wave function with only the first higher-order component generated is given by

$$g(t - x_0/v_s) = C \text{ rect}[(t - PW/2 - x_0/v_s - /2)/PW]$$

$$\cdot \exp[-j2\pi f_s(t - x_0/v_s - /2) - j\phi_0], \qquad (4)$$

where f_s is the carrier frequency, C is the pulse amplitude, and PW is the pulse width. The leading edge of the pulse arrives at $x_0 = -D/2$ at t=0 with phase ϕ_0.

With this modified configuration for spectrum analysis, the amplitude distribution of the signal in the frequency plane is obtained by substituting Eqs. (2) and (4) into Eq. (1) and solving the integral in terms of error functions [7], we have

$$U_1(x_1, y_1, t) = K \delta(y_1) \int_{-\infty}^{\infty} g(t - x_0/v_s)\, w(x_0) \exp(-j2\pi u x_0)\, dx_0$$

$$= K C \delta(y_1)/2 \exp[-j2\pi f_s(t - /2) - /2]$$

$$\cdot (\pi/a)^{\frac{1}{2}} \exp(b^2/a) \left[\text{erf}(a^{\frac{1}{2}} B + b/a^{\frac{1}{2}}) \right.$$

$$\left. - \text{erf}(a^{\frac{1}{2}} A + b/a^{\frac{1}{2}}) \right] \qquad (5)$$

where

$$a = (2Tx/D)^{\cdot} ,$$

$$b = j^{-}[u - f_S/v_S - j^{\cdot}/(2^{-}D)],$$

$$K = K_B/(^{\cdot}F)^{\frac{1}{2}} ,$$

B and A are the upper and lower limits, respectively, of the integral and they are a function of the pulse position in the aperture. For example, when only the leading edge of the pulse is in the aperture, the limits are defined by $A = -D/2$ and $B = -D/2 + v_S t$.

The optical illumination profile can be easily modified while the acoustic loss is inherent as it depends upon the material of the Bragg cell. Let us analyze the case where the laser illumination profile is uniform in the x dimension, to obtain insight on the characteristics of the field distribution. If the input signal is pulse-modulated with an amplitude C, then the amplitude distribution along the x_1 axis at $y_1 = 0$ can be expressed as

$$U_1(u,t) = K\ C\ \exp[-j2^{-}f_S(t - ^{\cdot}/2)]\ \exp(-\alpha^{\cdot}/2)$$

$$\cdot \int_{-\infty}^{\infty} \mathrm{rect}[(t - PW/2 - x_{\cdot}/v_S - ^{\cdot}/2)/PW]\ \mathrm{rect}(x_{\cdot}/D)$$

$$\cdot\ \exp\{-j2^{-}[u - f_S/v_S - j^{\cdot}/(2^{-}D)]\}\ dx_{\cdot} \qquad (6)$$

where the initial phase $^{\cdot}_0$ has been dropped from the above equation. There are four possible cases when considering a pulse-modulated cw signal and they are

(A) When the pulse fills up the aperture.
(B) Only the leading edge of the pulse in the aperture.
(C) Only the trailing edge of the pulse in the aperture and
(D) both the leading and trailing edges in the aperture.

These four cases will be considered in some details in this section.

2.1 The Pulse Completely Fills the Aperture

This is the only case for an input cw signal, but can also occur when using a pulsed signal which has a pulse width longer than the aperture transit time. In both cases, the limits of integration are now defined by the aperture, namely, $A = -D/2$ and $B = D/2$ and the amplitude distribution is

$$U_i(u,t) = C\ K\ D\ \mathrm{sinc}[uD - f_S - j\ \alpha/(2\ )]$$

$$\exp(-\ \alpha/2)\ \exp[-j2\ f_S(t - \ /2)] \qquad (7)$$

The last phase term shows that the light frequency is upshifted by the input signal carrier frequency f_S. The magnitude is directly proportional to the pulse amplitude C, and the aperture width D. It is also attenuated by an average exponential factor given at one half of the aperture transit time. The spatial amplitude distribution along the u axis is a complex sinc function which is defined by

$$\mathrm{sinc}\ [\ uD - f_S - j\ \alpha/(2\ )]$$

$$= \frac{\sin[\ (uD - f_S)]\ \cosh(-\ \alpha/2) + j\ \cos[\ (uD - f_S)]\ \sinh(-\ \alpha/2)}{[\ uD - f_S - j\ \alpha/(2\ )\ ]} \qquad (8)$$

It is to be noted that the sinc function with a complex argument is uncommon in the literature. However since it appears very often in this report and is in a much more compact form than the expression given on the right hand side, it will therefore be used.

The intensity of the distribution is proportional to the square of the absolute value of the sinc distribution. It can be shown that the maximum value of the sinc square function with a complex argument occurs at the normalized spatial coordinate of $u = f_S/v_S$.

The square of the normalized absolute sinc function is plotted versus the normalized variable uD for various acoustic loss values of S and is shown in Fig. 2. The location of the centroid is shifted by f_S and its magnitude is normalized to unity. S is the normalized effective pulse width which is that portion of the pulse inside the aperture normalized by the total aperture width D, and is unity in this case. As can be seen from the plot, the effect of acoustic attenuation on the intensity distribution is to smooth out the waveform by slightly broadening its main lobe, increasing its sidelobe levels and filling up its nulls.

The peak amplitude of the distribution is given by

$$U_{ip} = C\ K\ D\ \left[\ \frac{1 - \exp(-\ )}{\alpha}\ \right] \qquad (9)$$

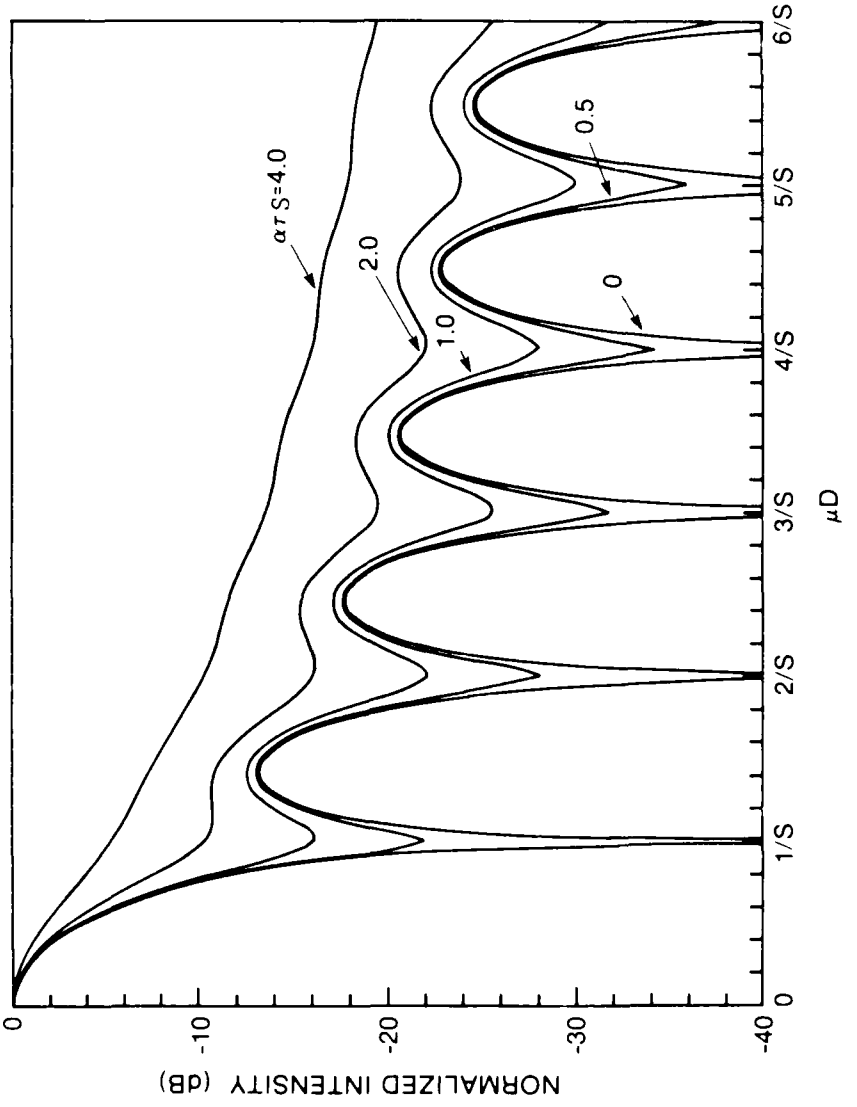

FIG. 2: NORMALIZED PLOT OF $\{[\sin\{[\mu D - j\alpha r/(2\pi)]S\}]^2\}$ VERSUS μD

The square of the last term is plotted in Fig. 3 as a function of . The normalized intensity distribution is plotted in Fig. 2, with its peak value normalized to unity, while the absolute value of the peak is plotted in Fig. 3. By using the plots of both Figs. 2 and 3, a semi-graphical technique can be used to obtain the absolute light intensity distribution as a function of and S.

In the limit when the loss is negligible, the amplitude distribution is simply given by the familiar sinc function

$$U_1(u,t) = C\ K\ D\ \mathrm{sinc}(uD - f_S\tau\ )\ \exp[-j2\pi f_S(t - \tau/2)] \tag{10}$$

2.2 Only the Leading Edge of the Pulse in the Aperture

In this case, the lower limit of integration is defined by the aperture boundary at A = -D/2 and the upper limit by the leading edge of the pulse, which is moving in time, that is,

$$B = -D/2 + v_S t\ ,\quad t < PW,\quad \tau \tag{11}$$

The amplitude distribution in the back focal plane is now

$$U_1(u,t) = K\ C\ D\ S\ \exp(-\pi\tau S/2)\ \mathrm{sinc}\{[uD - f_S\tau - j\pi\tau/(2\pi)]S\}$$
$$\cdot \exp\{-j\pi[(uv_S + f_S)t - uD]\} \tag{12}$$

where the normalized effective pulse width S = t/. The temporal frequency is given in the last exponential term as

$$f = (uv_S + f_S)/2 \tag{13}$$

The spatial amplitude distribution is again a complex sinc function as in the case of a cw signal except that it is a function of the effective pulse width. The temporal frequency at the centroid of the distribution ($u = f_S/\tau$) is also upshifted by the signal carrier frequency. However as we move away from the centroid, the temporal frequency varies continuously as u varies. At some incremental spatial frequency of u from the centroid, the temporal frequency deviation is $f_S/2$. The explanation for this phenomenon is that in this case, one edge moves, and the other one is stationary. The absolute square of the normalized sinc function is plotted in Fig. 2.

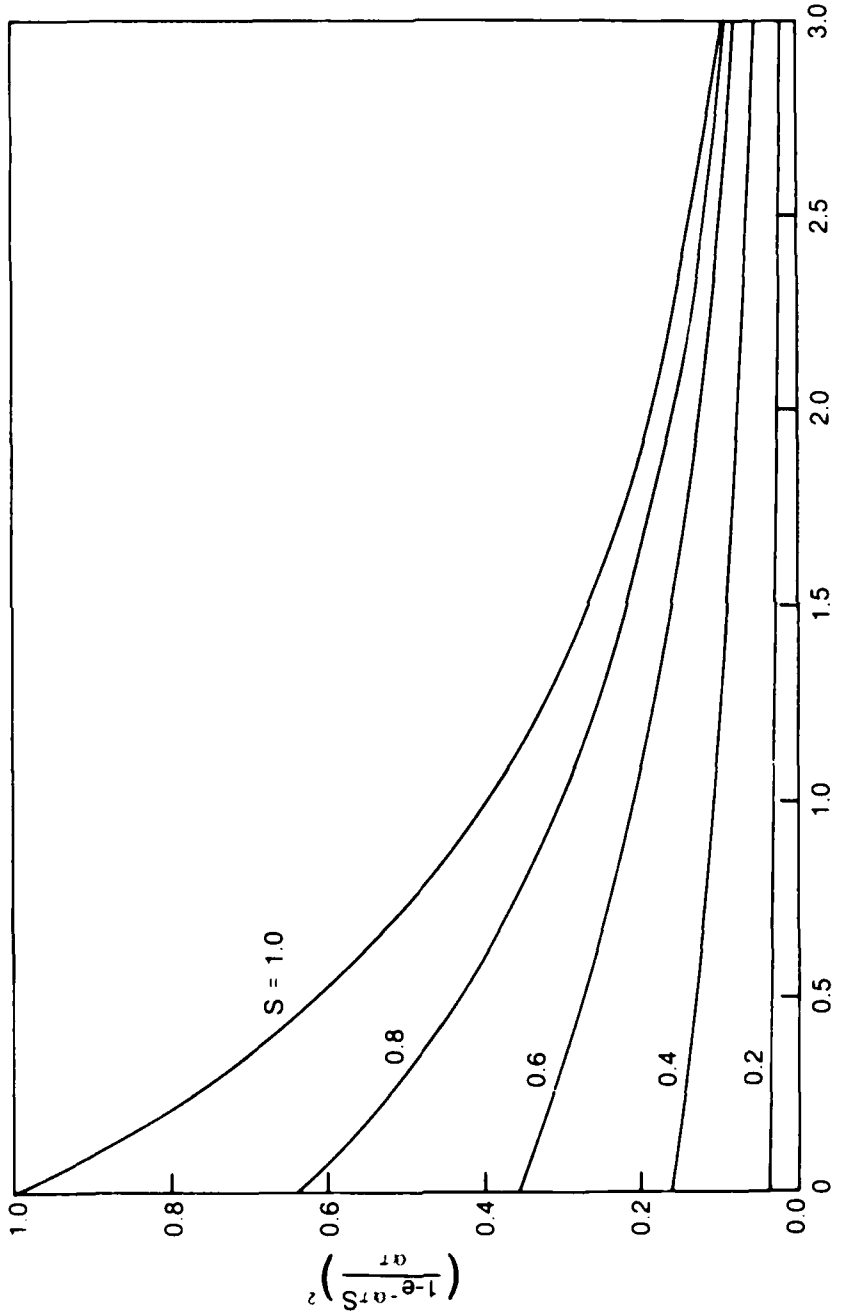

FIG. 3: PLOT OF $\{[1 - \exp(-\alpha TS)]/(\alpha T)\}^2$ VERSUS αT

As t increases, the effective pulse width increases proportionally and the magnitude of the centroid increases while its spatial width decreases. The peak amplitude of the centroid is given by

$$U_{cp}(t) = C\,K\,D\left[\frac{1-\exp(-\alpha\tau S)}{\alpha\tau}\right] \tag{14}$$

and the square of the bracketed term is plotted in Fig. 3.

2.3 Only the Trailing Edge of the Pulse in the Aperture

The upper limit is now defined by the aperture at B = D/2. The trailing edge of the pulse is moving in time and defined by

$$A = -D/2 + v_s(t - PW) \quad , \; 0 < t - PW < \tau \tag{15}$$

The amplitude distribution in the back focal plane is

$$\begin{aligned} U_1(u,t) = {} & K\,C\,D\,S\exp[-\alpha\tau(1-S)]\exp(-\alpha\tau S/2) \\ & \cdot \mathrm{sinc}\{[uD - f_s\tau - j\alpha\tau/(2\pi)]S\} \\ & \cdot \exp\{-j\pi[(uv_s + f_s)t - f_s\tau - (uv_s - f_s)PW]\} \end{aligned} \tag{16}$$

and $$S = 1 - (t - PW)/\tau \tag{17}$$

As expected, the distribution is of the same form as for the leading edge case. The only difference is that the amplitude is attenuated more for the same effective pulse width since it is now located at the exit end of the aperture. The peak amplitude of the centroid is

$$U_{cp}(u,t) = K\,C\,D\exp[-\alpha(t - PW)]\{[1 - \exp(-\alpha\tau S)]/(\alpha\tau)\} \tag{18}$$

2.4 Both the Leading and Trailing Edges in the Aperture

This case happens only when the pulse width PW is shorter than the aperture transit time τ. Both the leading and trailing edges are moving in time, that is,

$$A = -D/2 + v_s(t - PW)$$

$$B = -D/2 + v_s t \qquad (19)$$

for $0 < t - PW < \tau$

The amplitude distribution in the back focal plane is

$$U_i(u,t) = K\ C\ D\ S \exp[-\alpha(t - PW)] \exp(-\alpha\tau\ S/2)$$
$$\text{sinc}\{[uD - f_s\tau - j\alpha\tau/(2\pi)]S\}$$
$$\exp\{-j\pi[2uv_s t + (f_s - uv_s)PW - uD]\} \qquad (20)$$

and $$S = PW/\tau \qquad (21)$$

The temporal frequency is now

$$f = uv_s \qquad (22)$$

It varies continuously as a function of the normalized spatial frequency u. At the centroid, the temporal frequency is again equal to f_s. At some incremental frequency Δu away from the centroid, we find that the temporal frequency of the sidelobes differs from the centroid by Δf. The explanation for this phenomenon is that now both the leading and trailing edges move.

The spatial distribution is a complex sinc function with its magnitude decreasing with time. The square of the absolute value of the sinc function is given in Fig. 2. The amplitude of the centroid is

$$U_i(t) = K\ C\ D \exp[-\alpha(t-PW)]\{[1-\exp(\alpha\tau\ S)]/(\alpha\tau)\} \qquad (23)$$

The square of the last term is plotted in Fig. 3 as a function of $\alpha\tau\ S$.

3.0 DETECTION SCHEME

In power spectrum analyzers, the intensity distribution along the x_i axis as a function of time is of interest. For a given pulse width, this distribution is completely characterized by Eq.(5) and is a function of only two parameters, Tx and $\alpha\tau$.

We have seen in the last section for Tx = 0 , the waveform distribution is rather complicated as it is a function of where the pulse is located in the aperture. With the additional parameter Tx , the power pattern is expected to be much more complex.

A typical case is used to illustrate the formation of the power spectral distribution of a pulsed signal as it propagates across the aperture. The weighting function parameters are Tx = 0.8 and τ = 0.4.

The plots shown in Fig. 4 are for the case where the normalized pulse width (PW/τ) is unity. The normalized instantaneous intensity distribution is plotted at five different positions as the pulse propagates through the aperture. Due to symmetry in the waveform distribution, only the right half of the waveform is plotted for each location and the spectral centroid is chosen to be located at the origin. As can be seen from the plots, the instantaneous intensity distribution changes with the pulse position in the aperture and is complicated in shape.

In the implementation of a spectrum analyzer, solid-state linear photodetector arrays are usually used for detection. They operate either in the real-time mode with parallel individual outputs or in a time-integrating mode where the output is from detectors arrayed in serial/parallel configurations. In the time-integrating mode, there is a trade-off between the frequency resolution and the integration time for a given data rate. If a large number of photodetectors are used to obtain a fine resolution of the spectrum, the integration time is usually increased due to finite clock rates. In the real-time mode of operation, the number of photodetectors used must be limited to keep the number of parallel channels to a manageable level.

The time-integrated waveform distributions for pulse-modulated cw signals has been addressed [3] and therefore will not be considered further in this report.

In the real-time mode of operation, one is more interested in the instantaneous spectrum of the signal detected by the photodetector array. Using this accurate measurement of the output voltage from the photodetector array as a function of time, not only the pulse repetition frequency (PRF) but also the pulse width (PW) of the signal can be determined.

In general, the output voltage from a given photodetector is a function of the frequency response of the photodetector and the portion of the intensity distribution sampled by it. To keep the number of possible cases to a minimum, the most commonly employed 1/D bandwidth detection scheme is investigated. In this photodetector array configuration, the spectrum analyzer is used mainly as a frequency channelizer in which multiple simultaneous signals of different frequencies can be spatially separated. In this case, a coarse frequency resolution is obtained while the time resolution is very good.

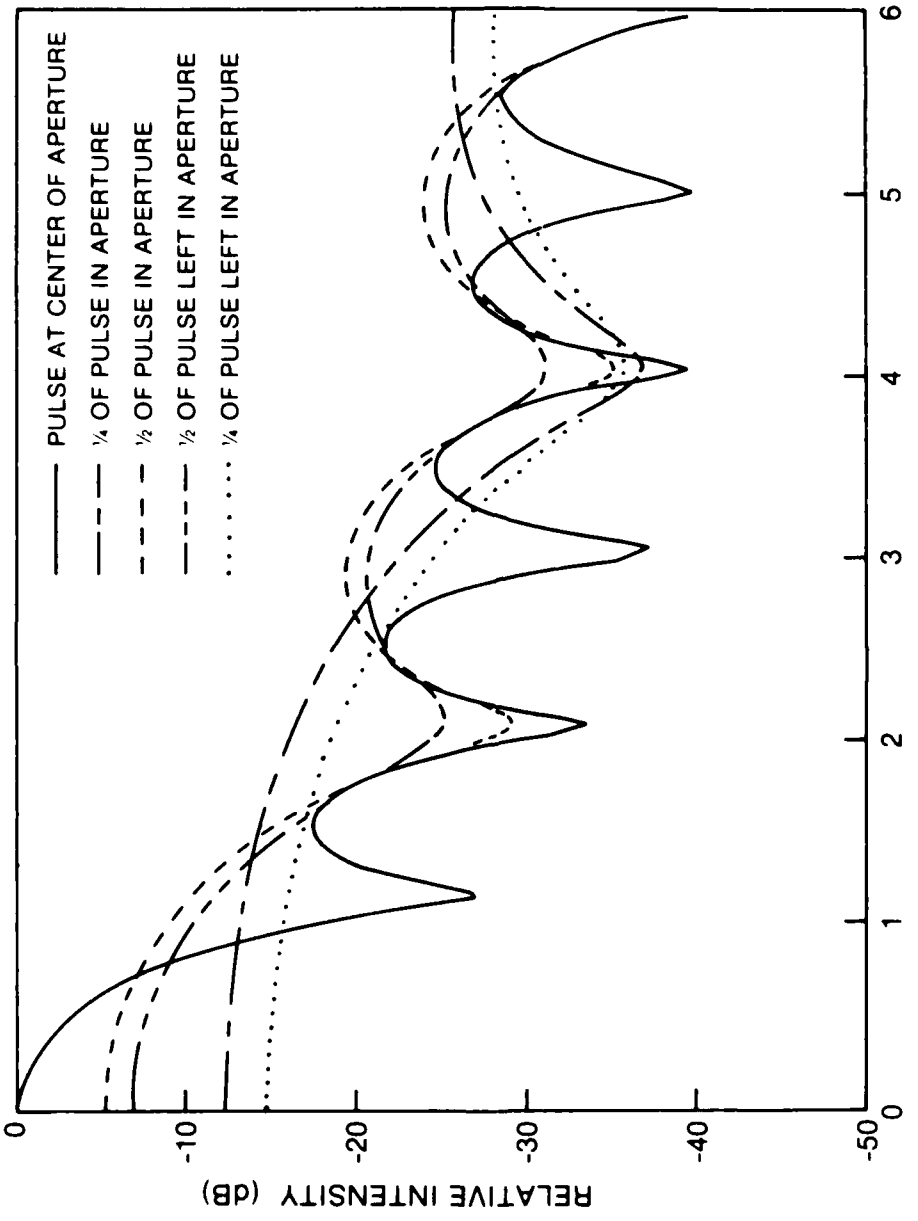

FIG. 4: RELATIVE LIGHT INTENSITY DISTRIBUTIONS AT FIVE DIFFERENT TIME INTERVALS: (PW/τ = 1.0, Tx = 0.8, and $\alpha\tau$ = 0.4)

4.0 1/D BANDWIDTH DETECTION

In this scheme of detection, the spectrum analyzer is configured in such a way that the photodetector width has a normalized spatial bandwidth equal to the reciprocal of the aperture width (D). If we designate the photodetector where the spatial distribution of the signal is approximately centered at K = 0, the output voltage from the Kth photodetector is

$$V_K(t) = \int\int U_i(u,v,t)\, H\left[\frac{u - (u_S + K\,\Delta u + u_\eta)}{\Delta u}, \frac{v}{\Delta v}\right] du\, dv * h(t) \qquad (24)$$

where H is the spatial weighting function of the photodetector array; $\Delta u = 1/D$ is the center-to-center spacing, Δv is the height of the photodetector array, $u_S = f_S/v_S$ is the location of the signal spectral centroid, u_η is the mismatch between the spectral centroid and the centered photodetector, h(t) is the impulse response of the detection circuit which normally consists of a photodetector followed by an amplifier, and * denotes convolution.

If the bandwidth of the detection circuit is much larger than the electrical bandwidth of the sampled waveform by the photodetector, the impulse response can be approximated by the delta function $\delta(t)$.

A simple case is used to illustrate the detected waveform characteristics with the weighting parameters $T_x = u_\eta = 0$ and a normalized pulse width (PW/Δ) of unity. It was carried out experimentally using a slit with a normalized spatial bandwidth of 1/D placed in front of a large photodetector. The slit with the photodetector was initially centered on the centroid of the signal spectrum and was then moved in steps of 1/(2D) away from it. The reason for the 1/(2D) step (half of the photodetector width) is to simulate the two extreme relative positions of the photodetector array with respect to the centroid of the signal spectrum. One case is when the spectral centroid is centered with respect to one of the photodetectors and the photodetectors on that array are designated by n = 2K = even integers. The other case is when the spectral centroid is located in between two adjacent photodetectors with n = 2K = odd integers.

The theoretical and experimental waveforms at the various photodetector locations are plotted in Figs. 5 and 6, respectively. The bandwidth of the detection circuit is much larger than the detected signal bandwidth and h(t) is approximated by the delta function $\delta(t)$. The spatial weighting function of the photodetector in this arrangement is of rectangular form. The photodetector located at the centroid of the spectrum is designated by n = 0, and all the curves are normalized by the maximum output value at n = 0 and $t/\Delta = 1$. In Fig. 5, only the first half of the response is plotted because the output waveform is symmetrical for the rectangular weighting function. In Fig. 6(b), the four experimental curves are displaced vertically by one division from each other to show a clearer picture.

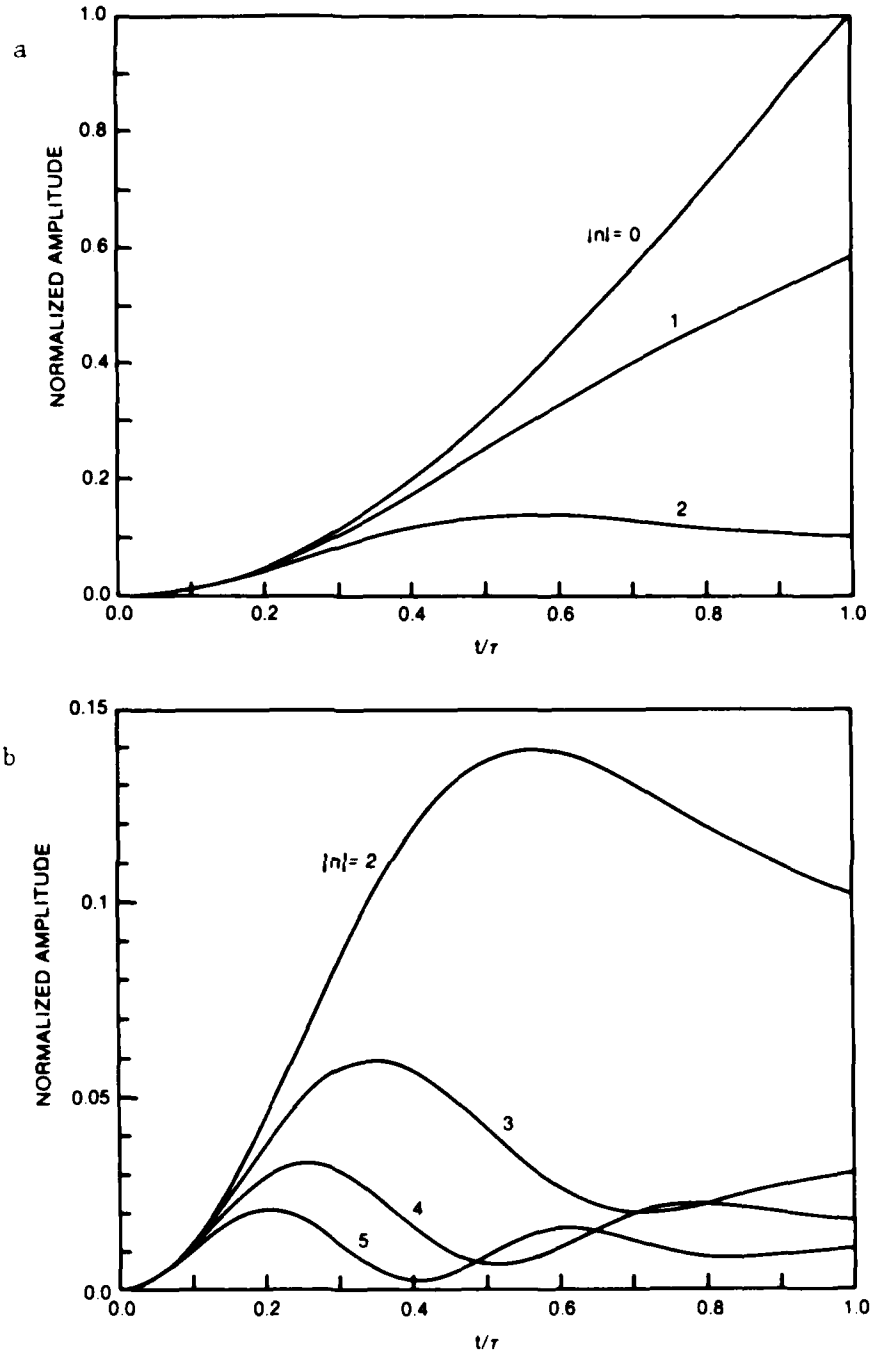

FIG. 5: 1/D BANDWIDTH DETECTION OF A PULSED SIGNAL VS PHOTODETECTOR LOCATION [n/(2D)] FROM THE SIGNAL CENTROID: (PW/ = 1.0, Tx = = 0), (a) |n| = 0, 1, AND 2, (b) |n| = 2, 3, 4, AND 5.

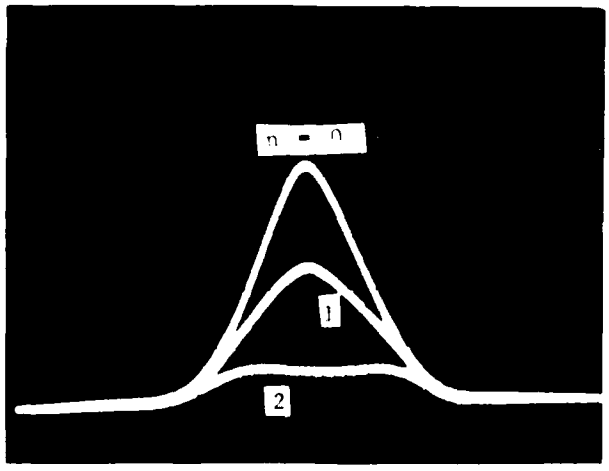

(a) n = 0, 1 and 2, 0.2 μsec/division

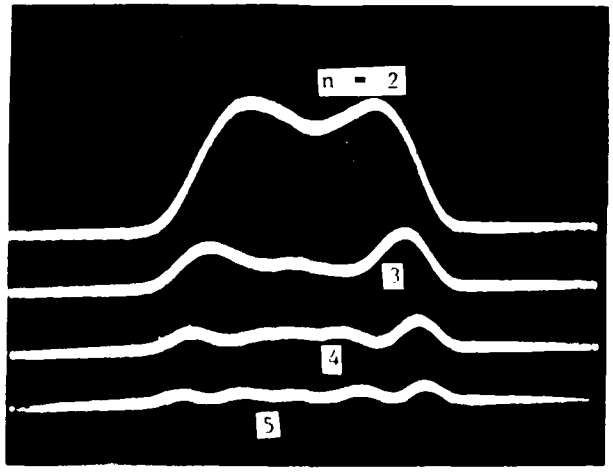

(b) n = 2, 3, 4 and 5, 0.2 μsec/division

FIG. 6: EXPERIMENTAL 1/D BANDWIDTH DETECTION OF A PULSED SIGNAL VS PHOTODETECTOR LOCATION [n/(2D)] FROM THE SIGNAL CENTROID: (PW/ = 1.0, PW = 0.625 s, Tx = = 0)
(a) n = 0, 1, AND 2, 0.2 s/div,
(b) n = 2, 3, 4 AND 5, 0.2 s/div.

For the rectangular weighting function, with Tx = α = 0, the power spectral distribution is always of the sinc squared function. Its magnitude increases with the square of the effective pulse width in the aperture while its main lobe width decreases proportionally to it. The minimum main lobe width is reached when the pulse completely fills the aperture, with its first nulls located at $u = \pm 1/D$ from the centroid and the other nulls spaced at 1/D apart.

In the case where $|n| = 0,1$, the photodetector is always situated inside the main lobe of the spectrum and, as a result, the detected output increases monotonically as the pulse enters the aperture. It reaches a maximum level when the pulse completely fills the aperture and then decreases to zero in the same fashion as the pulse leaves the aperture.

On the other hand, for a photodetector situated in other locations, it is initially located inside the main lobe of the spectrum as the pulse enters the aperture and the detected output increases with time. As the pulse moves in further, the nulls start moving in closer toward the centroid; every time a null crosses the photodetector, a dip in the output magnitude occurs and thus gives rise to the appearance of a hump in the detected waveform.

The number of humps appearing on the detected waveform from the nth photodetector is $|n|$ for $n \neq 0$. For example, if $|n| = 4$, the output registers four humps as the pulse propagates through the aperture, and with a maximum level of only 14.8 dB below that of the photodetector located at the spectral centroid.

So far we have only considered the cases where the spectral centroid is located either at the center or in between two photodetectors. However, in a practical situation, the spectral centroid of a given signal may be located anywhere along the photodetector array. When this happens, the magnitude and the number of humps appearing on the detected output will be slightly different from the above two cases, and they will fall somewhere in between.

As can be seen from the graphs in Fig 5., the maximum output from the photodetector array has only one peak (without the multiple-hump structure) appearing on the waveform. In the case where the spectral centroid is located in between two adjacent photodetectors, there are two identical maximum outputs. In all the other cases, there is only one such maximum output. If the weighting function is not a rectangular one, its effect on the instantaneous spectrum is to broaden the main lobe and to alter the sidelobe levels and spacings. This effect increases in direct proportion to the amount of overlapping between the pulse signal and the aperture. The broadening effect will move the first nulls further away from the centroid thus ensuring that there is at least one maximum output with only one peak appearing on the waveform. The change in the sidelobe levels and spacings will affect the shape and the number of humps detected by those photodetectors located off the signal spectral centroid.

The effect of the weighting parameters on the detected waveform is illustrated in Fig. 7. The detected waveform is taken from the photodetector which is centered with respect to the spectral centroid. For each set of weighting parameters, the response is plotted for two normalized pulse widths of PW/ = 0.5 and 1. The maximum response is normalized to a value of unity. As can be seen from the graph, the shape of the detected waveform is a strong function of the weighting function parameters.

The response for other pulse widths can also be derived from Fig. 5 when the weighting function is of the same rectangular form. If the normalized pulse width is greater than unity by t/ , the waveform at t/ = 1.0 will remain at that level for the same time duration. On the other hand, if the normalized pulse width is less than unity by t/ , the waveform will only reach the level at 1 - t/ and remain at that level until t/ equals unity. It will then retrace the waveform from t/ = (1 - t/) back to t/ = 0.

In all the discussions presented so far, the impulse response of the detection circuit is approximated by the delta function (t) . If the bandwidth of the detection circuit is not much larger than the detected signal bandwidth, the exact output waveform will depend on the bandpass nature of the detection circuit. It has the general effect of smoothing out the hump structure and stretching the output in time.

5.0 PULSE WIDTH DETERMINATION

As given in Eq. (24), the detected output waveform from a photodetector is a function of many parameters. It is in general a function of the pulse width, relative photodetector to spectral centroid location, spatial weighting function of the photodetector array, amplitude weighting function parameters, and the bandwidth of the detection circuit. The first two parameters are the unknowns to be determined by the acousto-optic spectrum analyzer. However, there are two characteristics which are independent of the above parameters, namely, (i) the input pulse width of the signal is stretched by an amount equal to the aperture transit time, and (ii) if the pulse width exceeds the aperture transit time by T , the detected output reaches a maximum level for the same duration T .

The above two characteristics can be utilized to determine the pulse width of an input signal. Let us take a signal scenario where there may be simultaneous signals present but non-overlapping in the frequency plane. The first function performed by the post-processor is to identify the photodetector output where the signal spectral centroid is located. This is obtained simply by finding the maximum photodetector output free of the multiple-hump structure. The second function is to determine the pulse width from this maximum output.

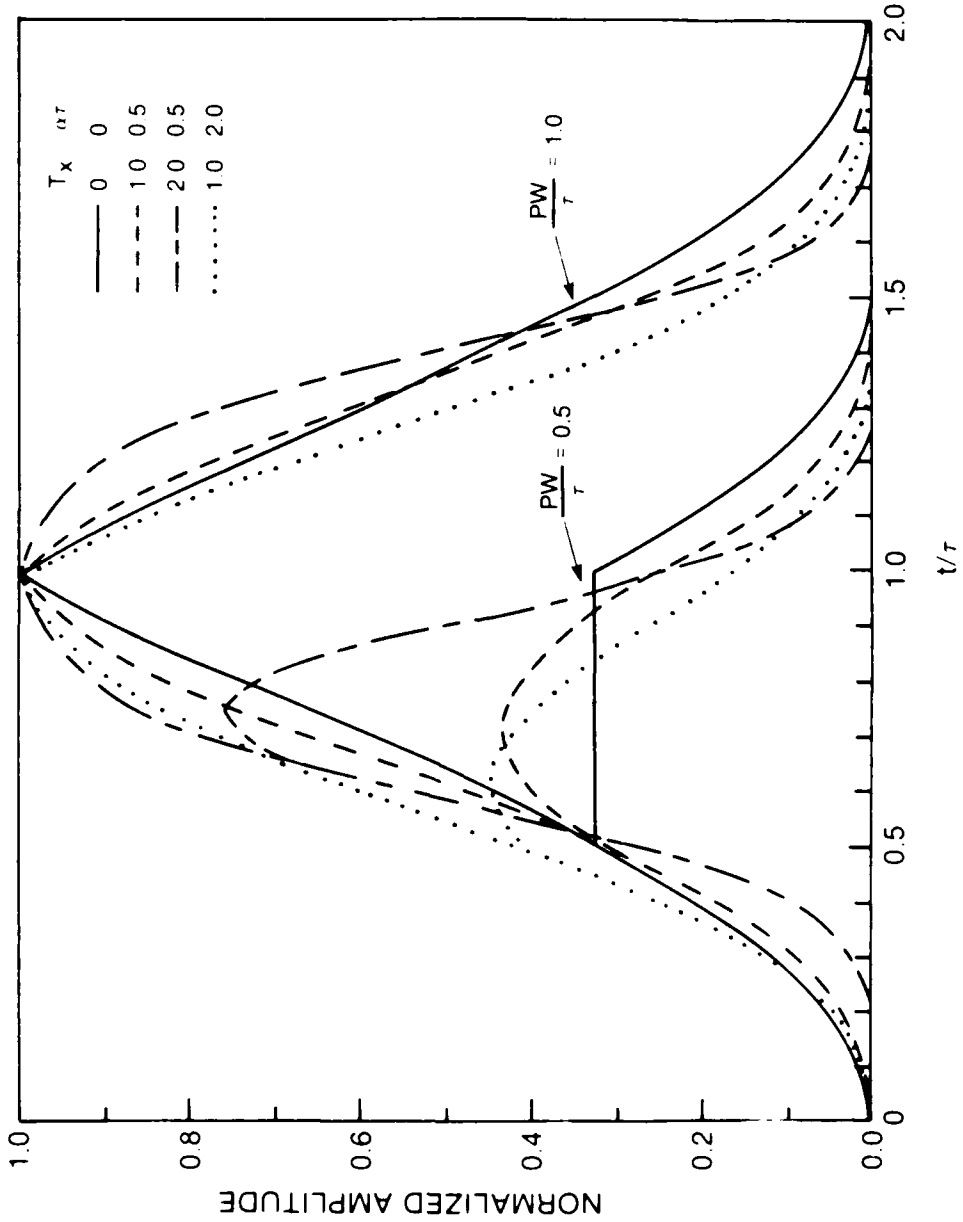

FIG. 7: 1/D BANDWIDTH DETECTION OF EQUIPOWER PULSED SIGNALS AS A FUNCTION OF THE WEIGHTING PARAMETERS: (PW/τ = 1.0 AND 0.5)

One approach is to make use of characteristic (i) where the pulse width is stretched by the aperture transit time,

$$T = PW + \qquad (25)$$

The pulse width can be estimated by measuring the duration of the detected signal and then subtracting from it the aperture transit time. This can be done by setting a certain threshold level above the noise floor to determine both the leading and trailing edges of the signal. It is apparent that this scheme works well for output signals with a large signal-to-noise ratio where both the leading and trailing edges are clearly defined. The measured pulse width becomes shorter as the signal-to-noise ratio decreases. If the parameters of the weighting function are large, the effective aperture transit time is reduced and an adjusting factor has to be used. Furthermore, if the impulse response of the detection circuit cannot be approximated by the delta function, the output waveform will be stretched further and an additional adjusting factor must be used.

Another approach to determine the pulse width is to make use of the second characteristic. If the pulse width exceeds the aperture transit time by ΔT, the detected output increases initially until a maximum level is reached when the pulse fills the aperture. The output stays at this maximum level for the same time duration ΔT and then decreases to zero as the trailing edge of the pulse leaves the aperture. The pulse width of the input signal is related to ΔT by

$$PW = \Delta T + \qquad (26)$$

To ensure that there is always a flat maximum region in the output of the detected waveform, the aperture transit time must be chosen shorter than the narrowest pulse width to be detected. This is not a serious constraint and it actually turns out to be what can be achieved in practice for broadband receiver applications. A Bragg cell with a bandwidth of 1 GHz has a limited useful aperture width due to high acoustic loss arising from operating in the higher frequency range. The input laser beam is confined to the region closest to the transducer to achieve a high diffraction efficiency. In addition, the number of parallel outputs must be limited in this mode of operation and thus fine frequency resolution is not required. A coarser frequency resolution means a shorter aperture transit time.

For example, if the aperture transit time is 0.25 s, any pulse width exceeding that value will have a flat maximum level in the detected output. This aperture will give a spot size equivalent to a frequency resolution of 4 MHz.

In a practical situation, both approaches to pulse width determination can be employed to take advantage of the merits each one has to offer.

In a real environment, the amplitude of the received pulse may be distorted. Both the rise and fall times are of finite duration. Moreover, the pulse amplitude is usually corrugated with ripples. These perturbations will in general distort the shape of the detected waveform and increase both the rise and fall times.

The ripples are usually small in amplitude and have a higher spatial frequency content than the pulse envelope. The power intercepted by the photodetector depends on the frequency components of the ripples. In general, there is an averaging effect applied to those spatial components falling within the photodetector's spatial bandwidth. This will in turn contribute some distortions to the detected output and affect the shape of the maximum flat region. However, these distortions are small in amplitude in comparison with the rising and falling edges of the detected output and can be taken into account by the postprocessor. If the spatial components fall outside the photodetector of interest, they will not affect the output but will contribute to the outputs of the adjacent photodetectors.

6.0 SUMMARY AND CONCLUSIONS

The temporal and spatial characteristics of the acousto-optic spectrum analyzer for pulse-modulated cw signals, have been investigated. In the case where the window weighting function contains only the acoustic exponential attenuation function, the spatial distributions have been shown to be characterized by a combination of exponential and complex sinc functions. The instantaneous spectral distribution generated by the spectrum analyzer as the pulse propagates through the Bragg cell aperture, is detected by using a photodetector array operating in the real-time mode. The center-to-center element spacing used in the analysis and measurements, has a normalized spatial bandwidth equal to the reciprocal of the aperture. This configuration is mainly used as a frequency channelizer in which a coarse frequency of the signal is obtained while the time resolution is very good. The detected signal waveform has been studied as a function of pulse width, amplitude weighting function parameters, and relative spectral centroid to photodetector location.

It was observed that the input pulse envelope is modified by the acousto-optic spectrum analyzer in a number of ways. It is always stretched in duration by an amount equal to the aperture transit time. Moreover, in the case where the pulse width is longer than the aperture time, the difference in duration was found to appear as a flat top on the detected output. The shape of the detected waveform is strongly affected by the amplitude weighting parameters. Furthermore, if the photodetector is located off the main lobe of the signal spectrum and detecting its sidelobes, multiple humps are detected.

However, despite the appearance of complicated waveform distributions, the first two characteristics, namely, the signal duration stretching and the duration of the maximum flat region were found to be simply related to the aperture transit time. This is especially true for the photodetector located at the spectral centroid where the output level is the highest and free of the multiple-hump structure. These two characteristics can then be utilized effectively in the determination of the pulse width.

7.0 REFERENCES

[1] D.L. Hecht, " Spectrum Analysis Using Acousto-optic Devices " , Optical Engineering, Vol. 16, No.5, pp. 461-466, Sept./Oct., 1977.

[2] A. Vander Lugt, " Bragg Cell Diffraction Patterns ", Applied Optics, Vol. 21, No. 6, pp. 1092-1100, 15 March, 1982.

[3] J.P.Y. Lee, " Acousto-optic Spectrum Analysis of Radar Signals Using an Integrating Photodetector Array ", Applied Optics, Vol. 20, No. 4, pp. 595-600, 15 Feb., 1981.

[4] A. Vander Lugt, " Interferometric Spectrum Analyzer ", Applied Optics, Vol. 20, No. 16, pp. 2770-2779, 15 Aug., 1981.

[5] L.C. Lennert, I.C. Chang, D.L. Steinmetz, W. Brooks and F. Langdon, "High-Performance GHz-Bandwidth Acousto-optic Spectrum Analyzer ", Proc. Soc. Photo-Opt. Instrum. Eng. 352, pp.10-16, Aug., 1982.

[6] J.P.Y. Lee and J.S. Wight, " Acousto-optic Spectrum Analyzer: Detection of Pulsed Signals ", Applied Optics, Vol. 25, No. 2, 15 Jan. 1986, pp.193-198.

[7] M. Abramowitz and I.A. Stegun, Handbook of Mathematical Functions, Dover, New York, 1965, p.556.

UNCLASSIFIED

Security Classification

DOCUMENT CONTROL DATA - R & D

(Security classification of title, body of abstract and indexing annotation must be entered when the overall document is classified)

1 ORIGINATING ACTIVITY
DEFENCE RESEARCH ESTABLISHMENT OTTAWA
DEPT. OF NATIONAL DEFENCE
SHIRLEY BAY, OTTAWA, ONTARIO K1A 0Z4

2a. DOCUMENT SECURITY CLASSIFICATION
UNCLASSIFIED

2b GROUP

3 DOCUMENT TITLE
"ACOUSTO-OPTIC SPECTRUM ANALYSER: TEMPORAL RESPONSE AND DETECTION OF PULSED SIGNALS (U)

4 DESCRIPTIVE NOTES (Type of report and inclusive dates)
DREO TECHNICAL NOTE

5 AUTHOR(S) (Last name, first name, middle initial)
LEE, JIM P.

6 DOCUMENT DATE	7a. TOTAL NO OF PAGES	7b NO. OF REFS
DECEMBER 1986	23	7

8a PROJECT OR GRANT NO	9a ORIGINATOR'S DOCUMENT NUMBER(S)
011LB11	DREO TN 87-5
8b CONTRACT NO	9b OTHER DOCUMENT NO (S) (Any other numbers that may be assigned this document)

10 DISTRIBUTION STATEMENT
UNLIMITED

11 SUPPLEMENTARY NOTES	12. SPONSORING ACTIVITY
	DREO

13 ABSTRACT

(U) This report describes the temporal response of an acousto-optic spectrum analyzer to pulse-modulated cw signals. The detected waveforms from the outputs of a real-time photodetector array are analyzed as a function of pulse width, weighting function parameters, and relative photodetector to spectral centroid location. The input pulse envelope is modified in the forms of signal duration stretching, the appearance of a flattop, multiple humps, and longer rise and fall times. Various schemes are discussed on the determination of the pulse width from the detected waveform.

DSIS

UNCLASSIFIED

Security Classification

KEY WORDS

ACOUSTO-OPTIC SPECTRUM ANALYZER
PULSEWIDTH DETERMINATION
ACOUSTO-OPTIC RECEIVER
BRAGG CELLS

INSTRUCTIONS

1 ORIGINATING ACTIVITY Enter the name and address of the organization issuing the document.

2a DOCUMENT SECURITY CLASSIFICATION Enter the overall security classification of the document including special warning terms whenever applicable.

2b GROUP Enter security reclassification group number. The three groups are defined in Appendix 'M' of the DRB Security Regulations.

3 DOCUMENT TITLE Enter the complete document title in all capital letters. Titles in all cases should be unclassified. If a sufficiently descriptive title cannot be selected without classification, show the classification with the usual one-capital-letter abbreviation in parentheses immediately following the title.

4 DESCRIPTIVE NOTES Enter the category of document, e.g. technical report, technical note or technical letter. If appropriate, enter the type of document, e.g. interim, progress, summary, annual or final. Give the inclusive dates when a specific reporting period is covered.

5 AUTHOR(S) Enter the name(s) of author(s) as shown on or in the document. Enter last name, first name, middle initial. If military, show rank. The name of the principal author is an absolute minimum requirement.

6 DOCUMENT DATE Enter the date (month, year) of Establishment approval for publication of the document.

7a TOTAL NUMBER OF PAGES The total page count should follow normal pagination procedures, i.e., enter the number of pages containing information.

7b NUMBER OF REFERENCES Enter the total number of references cited in the document.

8a PROJECT OR GRANT NUMBER If appropriate, enter the applicable research and development project or grant number under which the document was written.

8b CONTRACT NUMBER If appropriate, enter the applicable number under which the document was written.

9a ORIGINATOR'S DOCUMENT NUMBER(S) Enter the official document number by which the document will be identified and controlled by the originating activity. This number must be unique to this document.

9b OTHER DOCUMENT NUMBER(S) If the document has been assigned any other document numbers (either by the originator or by the sponsor), also enter this number(s).

10 DISTRIBUTION STATEMENT Enter any limitations on further dissemination of the document, other than those imposed by security classification, using standard statements such as:

(1) "Qualified requesters may obtain copies of this document from their defence documentation center."

(2) "Announcement and dissemination of this document is not authorized without prior approval from originating activity."

11 SUPPLEMENTARY NOTES Use for additional explanatory notes.

12 SPONSORING ACTIVITY Enter the name of the departmental project office or laboratory sponsoring the research and development. Include address.

13 ABSTRACT Enter an abstract giving a brief and factual summary of the document, even though it may also appear elsewhere in the body of the document itself. It is highly desirable that the abstract of classified documents be unclassified. Each paragraph of the abstract shall end with an indication of the security classification of the information in the paragraph (unless the document itself is unclassified) represented as (TS), (S), (C), (R), or (U).

The length of the abstract should be limited to 20 single-spaced standard typewritten lines; 7½ inches long.

14 KEY WORDS Key words are technically meaningful terms or short phrases that characterize a document and could be helpful in cataloging the document. Key words should be selected so that no security classification is required. Identifiers, such as equipment model designation, trade name, military project code name, geographic location, may be used as key words but will be followed by an indication of technical context.

END

6-87

DTIC